

arxiv文献泛读20210125-27

Revealing the cosmic reionisation history with fast radio bursts in the era of Square Kilometre Array

<https://arxiv.org/abs/2101.08798>

► details

Authors: Tetsuya Hashimoto, Tomotsugu Goto, Ting-Yi Lu, Alvina Y. L. On, Daryl Joe D.

Santos, Seong Jin Kim, Ece Kilerci Eser, Simon C.-C. Ho, Tiger Y.-Y. Hsiao, Leo Y.-W. Lin

Comments: Accepted for publication in MNRAS. A summary video is available at [this URL](#)

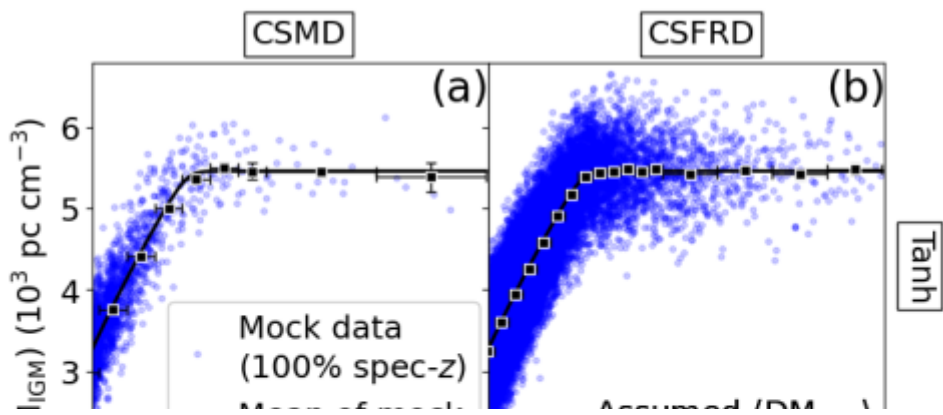
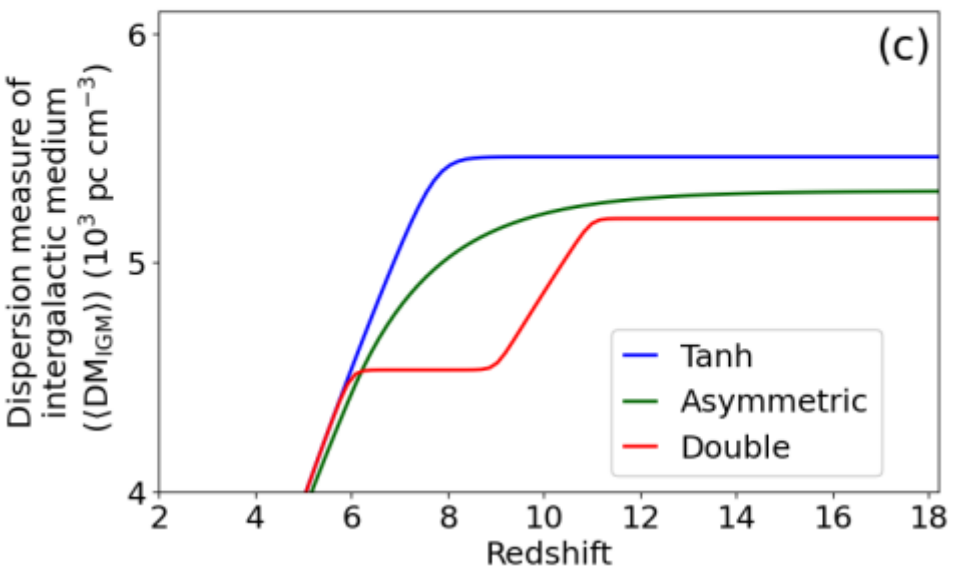
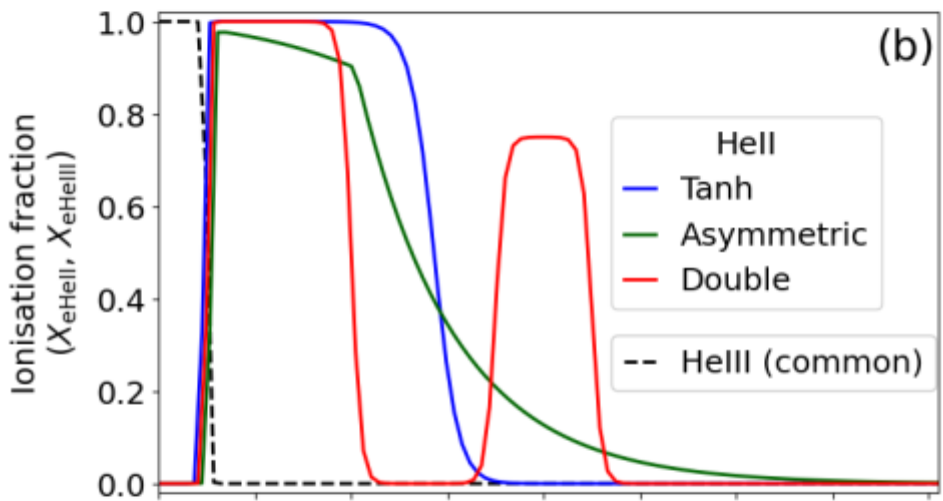
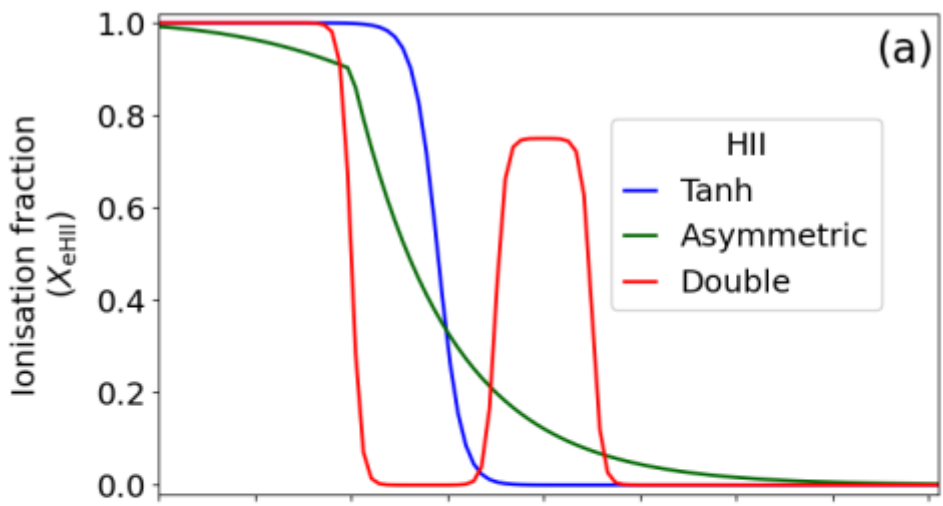
Revealing the cosmic reionisation history is at the frontier of extragalactic astronomy. The power spectrum of the cosmic microwave background (CMB) polarisation can be used to constrain the reionisation history. Here we propose a CMB-independent method using fast radio bursts (FRBs) to directly measure the ionisation fraction of the intergalactic medium (IGM) as a function of redshift. FRBs are new astronomical transients with millisecond timescales. Their dispersion measure (DMIGM) is an indicator of the amount of ionised material in the IGM. Since the differential of DMIGM against redshift is proportional to the ionisation fraction, our method allows us to directly measure the reionisation history without any assumption on its functional shape. As a proof of concept, we constructed mock non-repeating FRB sources to be detected with the Square Kilometre Array, assuming three different reionisation histories with the same optical depth of Thomson scattering. We considered three cases of redshift measurements: (A) spectroscopic redshift for all mock data, (B) spectroscopic redshift for 10% of mock data, and (C) redshift estimated from an empirical relation of FRBs between their time-integrated luminosity and rest-frame intrinsic duration. In all cases, the reionisation histories are consistently reconstructed from the mock FRB data using our method. Our results demonstrate the capability of future FRBs in constraining the reionisation history.

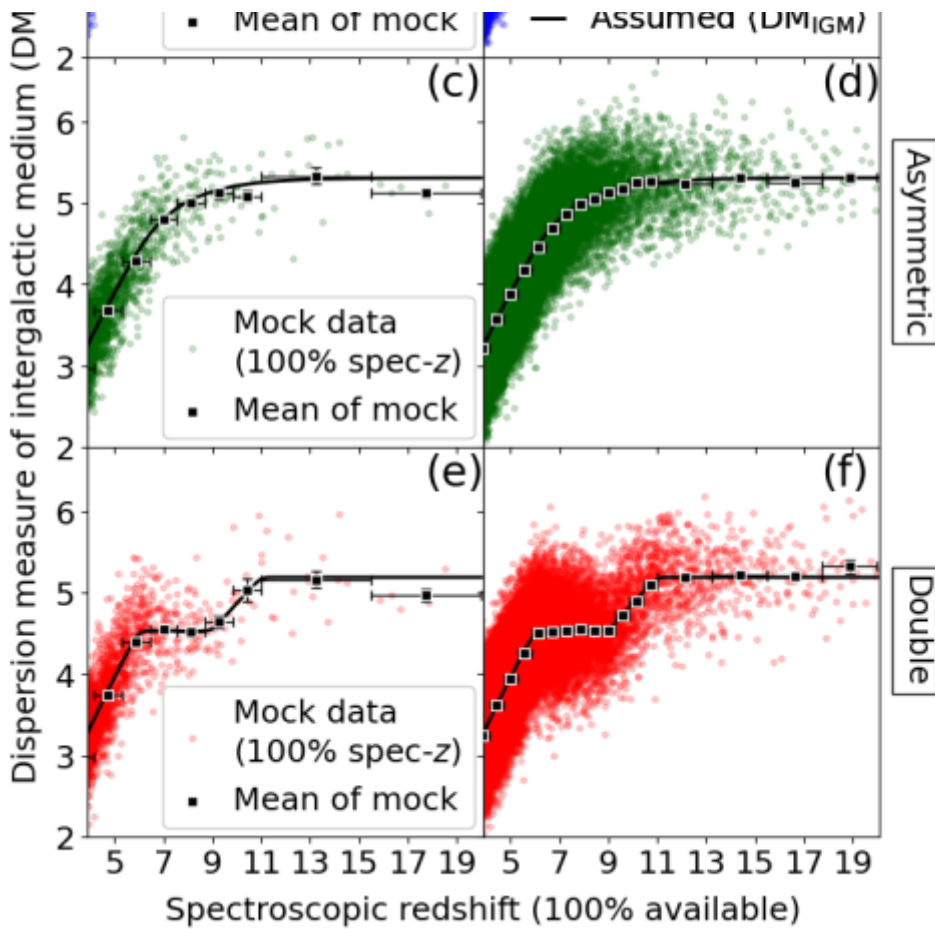
- 利用FRB研究宇宙再电离演化

In this work, we propose to differentiate the $\langle \text{DM}_{\text{IGM}} \rangle$ against redshift, i.e., $\frac{d\langle \text{DM}_{\text{IGM}} \rangle(z)}{dz}$, to measure $X_{\text{eH II}}$. At the hydrogen reionisation epoch, $X_{\text{eHe III}}$ can be approximated as $X_{\text{eH II}}$ (e.g., [Dai & Xia 2020](#)) because both neutral hydrogen and neutral helium are singly ionised by ionising photons radiated from star-forming galaxies. Supposing that the helium reionisation happened at $z \sim 3\text{-}4$ (e.g., [Becker et al. 2011](#)), $X_{\text{eHe III}} \sim 0$ at $z > 4$. Therefore, by differentiating Eq. 3 against redshift, $X_{\text{eH II}}$ at the hydrogen reionisation epoch is expressed as

$$X_{\text{eH II}}(z) = \frac{d\langle \text{DM}_{\text{IGM}} \rangle(z)}{dz} \frac{3H_0 c \Omega_b}{8\pi G m_p} \frac{1}{Y_{\text{H}} + \frac{1}{4}Y_{\text{p}}} \times \frac{\left\{ \Omega_m (1+z)^3 + \Omega_\Lambda (1+z)^{3[1+w(z)]} \right\}^{1/2}}{(1+z)f_{\text{IGM}}(z)}. \quad (5)$$

Since $\frac{d\langle \text{DM}_{\text{IGM}} \rangle(z)}{dz}$ will be measured by a slope in the $\text{DM}_{\text{IGM}}\text{-}z$ parameter space, Eq. 5 allows us to directly measure $X_{\text{eH II}}(z)$ without any assumption on a functional shape of the reionisation history. In the following sections, we demonstrate how this method can work in the SKA era using mock FRB data.





Spectroscopic monitoring of the candidate tidal disruption event in F01004-2237

<https://arxiv.org/abs/2101.09694>

► details

Authors: Giacomo Cannizzaro, Peter G. Jonker, Daniel Mata-Sánchez

Comments: 9 pages, 3 figures, 2 tables. Accepted for publication on ApJ on January 22, 2021

We present results of spectroscopic monitoring observations of the Ultra-Luminous Infra Red Galaxy F01004-2237. This galaxy was observed to undergo changes in its optical spectrum, detected by comparing a spectrum from 2015 with one from 2000. These changes were coincident with photometric brightening. The main changes detected in the optical spectrum are enhanced He II $\lambda 4686$ emission and the appearance of He I $\lambda 3898, \lambda 5876$ emission lines. The favoured interpretation of these changes was that of a tidal disruption event (TDE) happening in 2010. However, subsequent work suggested that these changes are caused by another hitherto unknown reason related to variations in the accretion rate in the active galactic nucleus (AGN). Our optical spectroscopic monitoring observations show that the evolution of the He lines is in line with the evolution seen in TDEs and opposite of what observed from reverberation mapping studies of AGNs, renewing the discussion on the interpretation of the flare as a TDE.

- 超亮红外星系F01004-2237 在2015年的光谱与在2000年的光谱相比发生了改变，主要变化是增强的He II $\lambda 4686$ 发射线 以及 He I $\lambda 3898, \lambda 5876$ 发射线的出现。
- 此变化也与其测光增亮相一致。
- 较有可能的解释是该变化由发生在2010年的TDE事件导致，但后续的一些工作表明这些变化是由与活动星系核中吸积率的变化相关的原因导致的。
- 作者对该源的光谱跟踪观测表明，He线的演化与已知TDE中观察到的演化一致，而与在AGN相关研究 (reverberation mapping studies) 中观察到的不一致。
- 因此这个耀发仍有可能是一个TDE。

-
- TDE的光谱演化应该是怎样的？AGN光谱应该是怎样的？
 - 为什么开始用TDE解释光谱变化？
 - 为什么否定TDE的解释而用AGN相关解释？
 - 为什么现在又转而支持TDE解释而否定AGN解释？
-

- Tadhunter et al. (2017)使用TDE解释观测上的变化

from September 2015 with one from February 2000 one finds that prominent spectral changes are; enhanced He II $\lambda 4686$ line emission; and the appearance of He I lines at $\lambda 3898, \lambda 5876$. The historical lightcurve from the Catalina Sky Survey (CSS, Drake et al. 2009) shows a clear brightening starting around 2010. This together with the spectroscopic changes led T17 to propose a TDE, triggered in 2010, as the explanation for the observed changes.

- 作者支持TDE的理由，以及TDE光谱演化的特征

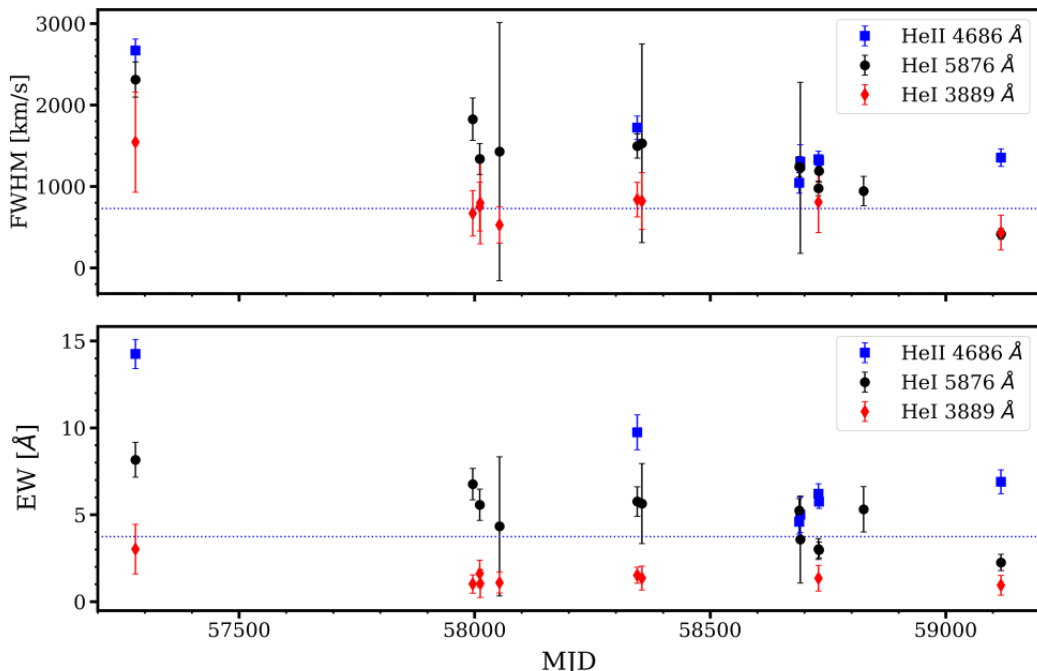


Figure 3. Results of the fits to the emission lines of He in our WHT and TGN spectra. Top panel: FWHM of He II $\lambda 4686$ (blue squares), He I $\lambda 5876$ (black circles) and He I $\lambda 3889$ (red diamonds). Bottom panel: EW of the same emission lines (with the same color/marker combination as the top panel). The dotted blue lines indicate the value of the He II line measured from the STIS spectra of 09 February 2000 (MJD 51584). The He I lines were not detected in that spectrum. On the X-axis, the Modified Julian Date of the observations.

- 1. 宽He线是TDE的普遍特征，特别是 He II λ 4686，尽管根据[Trakhtenbrot et al. 2019](#)，大部分TDE的He线宽度要大于F01004-2237光谱中的He宽度。

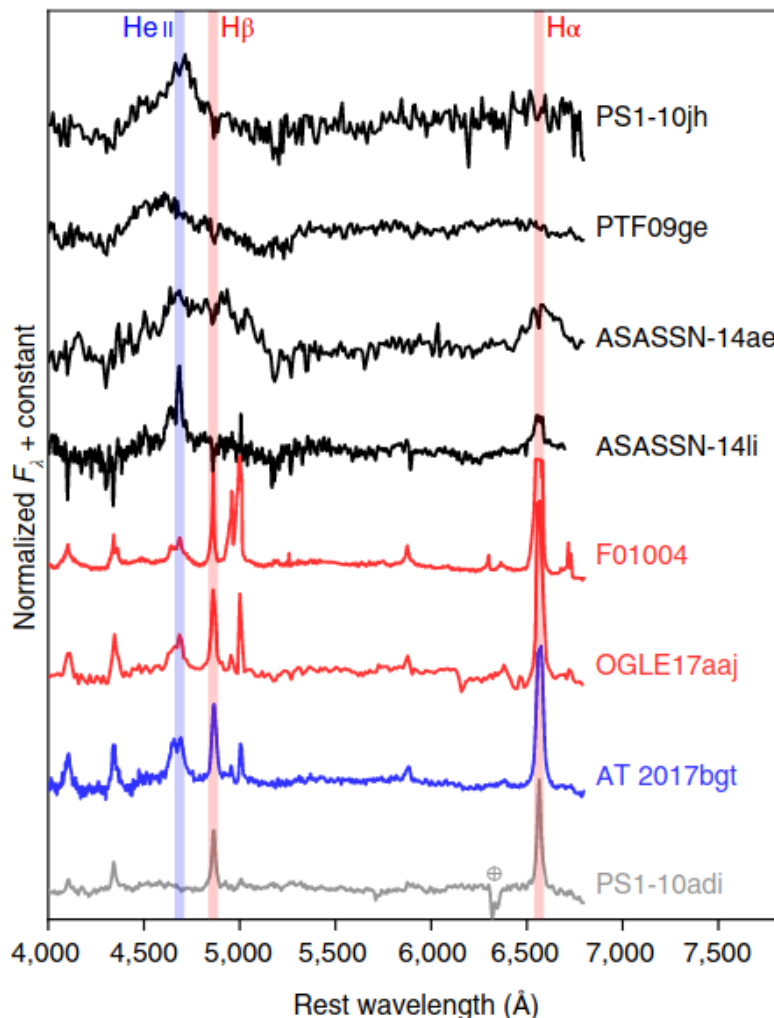


Fig. 4 | Broad emission features near He II λ 4,686 in AT 2017bgt, and similar objects, compared with other nuclear transients. Here we show the spectra of AT 2017bgt (in blue) and the recently reported events in F01004-2237 (ref. ²⁹) and OGLE17aaaj (refs. ^{31,32}; both in red), which we consider here to be part of a new class of nuclear transients. These are compared with spectra of four different TDEs (from refs. ²⁻⁵; in black), and

- 2.He II 和 He I λ 5876 的宽度 (FWHM, EW) 逐渐变小, 符合在其它TDE候选体中观察到的行为, 而不符合在AGN中观察到的行为: 随着光度减小, 线宽增大。

The presence of broad He emission lines is common in TDEs and especially a broad He II λ 4686 emission is considered a strong indicator of such phenomena (see van Velzen et al. e.g. 2020). However, while the FWHM of the He II λ 4686 emission line in F01004 can be called “broad”, in most TDEs the value of the FWHM is significantly larger than that observed in F01004 (cf. Trakhtenbrot et al. 2019). Nevertheless, as we showed in this paper, the evolution of its FWHM over time in F01004 is in line with what seen in other TDE candidates: the lines become narrower with time (Holoién et al. 2014; Brown et al. 2017; Onori et al. 2019) as the flare decays and the line EW becomes lower. This behaviour is opposite of that seen in AGNs, where reverberation mapping studies have shown that the lines become broader with decreasing source luminosity (e.g. Peterson et al. 2004). The evolution of the EW of the He lines follows a more shallow but similar decay.

- He线宽度的变化由中心黑洞吸积流的变化导致。

this scenario. Therefore, we conclude that the observed trends in the EW and FWHM of the He II and the He I line at λ 5876 is caused by changes in the accretion flow around the central supermassive black hole.

- T19 反对TDE解释的理由:

- 持续时间长, He II线不够宽

Their main argument for this is the long duration of the flare and the FWHM of the He II line, which is smaller than what commonly observed in TDEs (e.g Arcavi et al. 2014). Furthermore, the He lines in F01004 show a lower blue-shift than typically seen in TDEs, where the broad emission lines are often blue-shifted by several 1000's km s^{-1} (e.g. Nicholl et al. 2020). It is important to note

- 关于持续时间长 (~ 10 yr)，本文作者认为可能是受到F01004中的AGN的影响。

for the X-ray emission. So far, there is no reported optical emission that lasts this long. Perhaps, the presence of an AGN in F01004 could explain the decade-long signatures of a TDE. TDEs in AGNs are not well explored, but the interaction between the debris stream and the pre-existing accretion disk can significantly modify the canonical picture of a \sim year long decay (Chan et al. 2019).

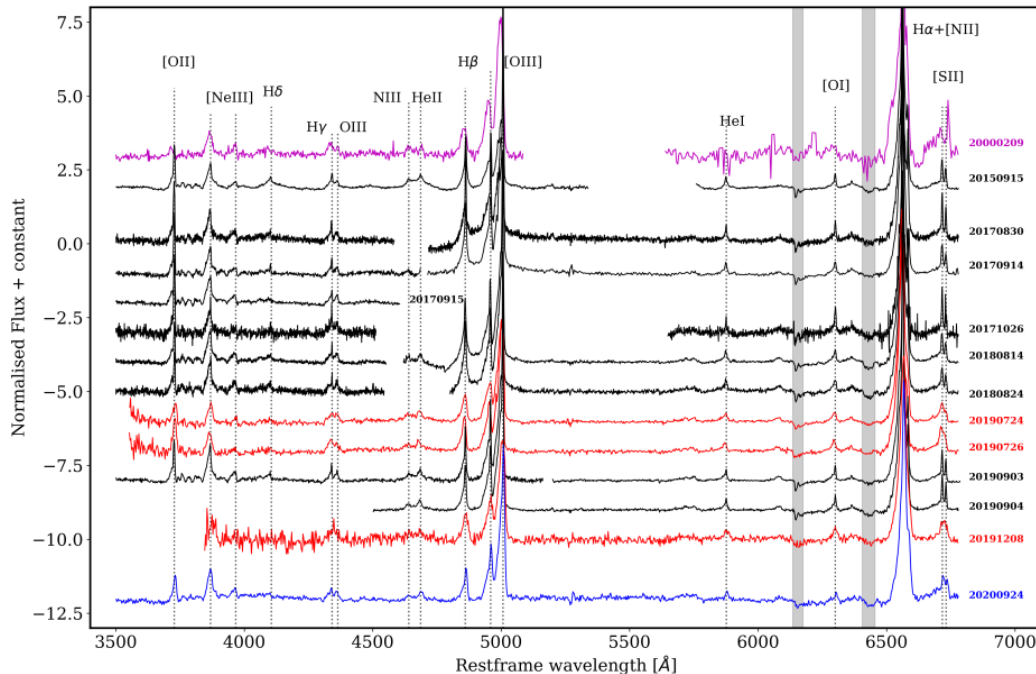


Figure 1. The sequence of spectra taken with HST/STIS (magenta), WHT/ISIS (black), WHT/ACAM (red) and TNG/DOLORES (blue) under study in this paper. For each spectrum the date of observation is given on the right hand side. The dotted lines indicate the wavelength of the main emission lines. The grey bands indicate wavelength ranges affected by telluric absorption. The spectra are not flux calibrated and the continuum has been normalised (see text for details).

- AGN的光谱特征：

- [O II] $\lambda 3727$, [Ne III] $\lambda 3869$, H δ , H γ , [O III] $\lambda 4363, \lambda 4959, \lambda 5007$, N III $\lambda 4640$, He II $\lambda 4686$, H β , He I $\lambda 3889, \lambda 5876$, [O I] $\lambda 6300$, H α , [N II] $\lambda 6548, \lambda 6584$ and [S II] $\lambda 6717, \lambda 6731$

The N III $\lambda 4640$ emission line is consistent with being caused by Wolf-Rayet stars (see T17 and references therein), as is the He II $\lambda 4686$ in the pre-flare HST spectrum. The rest of the emission lines are typically observed in AGNs. We fit the emission lines with a com-

Off-axis jet scenario for early afterglow emission of low-luminosity gamma-ray burst GRB 190829A

<https://arxiv.org/abs/2101.10581>

► details

Authors: Yuri Sato, Kaori Obayashi, Ryo Yamazaki, Kohta Murase, Yutaka Ohira

Comments: 9 pages, 4 figures

Recently, ground-based Imaging Atmospheric Cherenkov Telescopes have reported the detection of very-high-energy (VHE) gamma rays from some gamma-ray bursts (GRBs). One of them, GRB~190829A, was triggered by the Swift satellite, and about 20000 s after the burst onset the VHE gamma-ray emission was detected by H.E.S.S. with ~ 5 sigma significance. This event had unusual features of having much smaller isotropic equivalent gamma-ray energy than typical long GRBs and achromatic peaks in X-ray and optical afterglow at about 1400 s. Here we propose an off-axis jet scenario that explains these observational results. In this model, the relativistic beaming effect is responsible for the apparently small isotropic gamma-ray energy and spectral peak energy. Using a jetted afterglow model, we find that the narrow jet, which has the initial Lorentz factor of 350 and the initial jet opening half-angle of 0.015 rad, viewed off-axis can describe the observed achromatic behavior in the X-ray and optical afterglow. Another wide, baryon-loaded jet is necessary for the later-epoch X-ray and radio emissions. According to our model, the VHE gamma rays observed by H.E.S.S. at 20000 s may come from the narrow jet through the synchrotron self-Compton process.

- GRB 190829A 是由Swift触发的一个长爆，且在爆后~20000s，H.E.S.S探测到超高能的伽玛射线。
- 该爆主要特征是，其各向同性能量相对典型长爆来说很低，另外，X波段和光学波段的消色差拐折发生在大约1400s。
- 作者提出偏轴模型来解释观测特征：
 - 相对论集束效应导致看上去很小的各向同性能量，并且也能解释谱峰值能量。
 - $\Gamma_0 \sim 350, \theta_0 \sim 0.015\text{rad}(0.86^\circ)$ 的狭窄喷流的偏轴观测可描述X射线和光学余辉的拐折。
 - H.E.S.S在~20000s观测到的VHE伽玛射线可能来自喷流中的SSC过程。

-
- VHE E_γ ?
 - 该事件的 E_{iso} 与典型长爆的 E_{iso} ?
 - 20000s内有持续辐射？就光变曲线来看，应该是的。
 - 偏轴如何解释~1400s的拐折？
 - 跟踪观测情况？这篇文章应该没有自己观测，用的其他工作的数据。
-

- 该事件的 E_{iso} 与典型长爆的 E_{iso} ?

Compared with GRB 190114C and 180720B, GRB 190829A has some peculiar observational properties. The prompt gamma-ray emission (from ~ 10 keV to MeV band) consists of two temporally separated components (Chand et al. 2020). The burst started with less energetic emission (hereafter Episode 1 following Chand et al. 2020) with an isotropic equivalent gamma-ray energy of $E_{iso,\gamma} = 3.2 \times 10^{49}$ erg and a peak energy (that is, the photon energy at which the νF_ν -spectrum takes a maximum) $E_p = 120$ keV. After quiescent time interval lasting about 40 s, the second brighter emission (Episode 2) with $E_{iso,\gamma} = 1.9 \times 10^{50}$ erg and $E_p = 11$ keV, appeared. The observed values of $E_{iso,\gamma}$ and E_p of Episode 2 are consistent with Amati relation (Amati et al. 2002; Sakamoto et al. 2008), while those of Episode 1 are in the region of low-luminosity GRBs. Both Episode 1 and 2 have smaller $E_{iso,\gamma}$ and E_p than typical long GRBs, including the other VHE gamma-ray events, GRB 190114C and 180720B (e.g., Huang et al. 2020a). Indeed, GRB 190829A occurred so nearby with a redshift of $z = 0.0785$ that such weak prompt emissions could be observed.

Figure 1. Afterglow light curves in the X-ray (10¹⁸ Hz: red), optical (V-band: blue) and radio bands (1.3 GHz: orange, 15.5 GHz: green), which is compared with the observed data of GRB 190829A (X-ray: red points, V-band: blue triangles, 1.3 GHz: orange filled-circles, 15.5 GHz: green squares).

- 典型长爆大概在 $10^{51.55}$ erg量级左右。来自韶宇学长的统计。

- 20000s内有持续辐射？就光变曲线来看，应该是的。

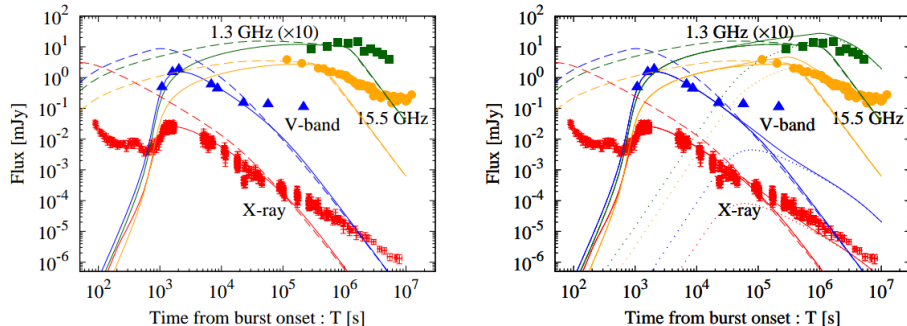


Figure 2. Afterglow light curves in the X-ray (10^{18} Hz: red), optical (V-band: blue) and radio bands (1.3 GHz: orange, 15.5 GHz: green), which is compared with the observed data of GRB 190829A (X-ray: red points, V-band: blue triangles, 1.3 GHz: orange filled-circles, 15.5 GHz: green squares). In the left panel, solid and dashed lines show the emission from the narrow jet ($\theta_0 = 0.015$ rad, $E_{iso,K} = 4.0 \times 10^{53}$ erg, $\Gamma_0 = 350$, $n_0 = 0.01 \text{ cm}^{-3}$, $\epsilon_e = 0.2$, $\epsilon_B = 5.0 \times 10^{-5}$ and $p = 2.44$), which is viewed off-axis ($\theta_v = 0.031$ rad) and on-axis ($\theta_v = 0$), respectively. In the right panel, we show the results of our two-component jet model — solid lines are the sum of the narrow (dashed lines) and wide (dotted lines) jets. The latter has parameters, $\theta_v = 0.031$ rad, $\theta_0 = 0.1$ rad, $E_{iso,K} = 2.0 \times 10^{53}$ erg, $\Gamma_0 = 20$, $n_0 = 0.01 \text{ cm}^{-3}$, $\epsilon_e = 0.4$, $\epsilon_B = 1.0 \times 10^{-5}$ and $p = 2.2$.

- 跟踪观测情况？这篇文章应该没有自己观测，用的其他工作的数据。

In this section, we show our numerical results of synchrotron afterglow emission in the X-ray (10^{18} Hz), optical (V-band), and radio (1.3 and 15.5 GHz) bands, and compare them with observation data of GRB 190829A. The X-ray data are extracted from the *Swift* team website¹ (Evans et al. 2007, 2009) which provides us with the integrated energy flux in the 0.3–10 keV band and the photon indices at some epoch. The index was around 2.2 at any time. On the other hand, we numerically calculate the energy flux density $F_{\nu=10^{18}\text{Hz}}$. In order to compare theoretical and observational results, we convert the observed integrated energy flux to the flux density at 10^{18} Hz assuming that the photon index is 2.2 at any time. The optical V-band data (before the absorption correction) are obtained from Chand et al. (2020). In our numerical calculation, we take the V-band extinction $A_V = 1.5$ mag (Chand et al. 2020). The radio data are taken from Rhodes et al. (2020).

- 偏轴如何解释~1400s的拐折？

- 使用了双喷流模型，原因？

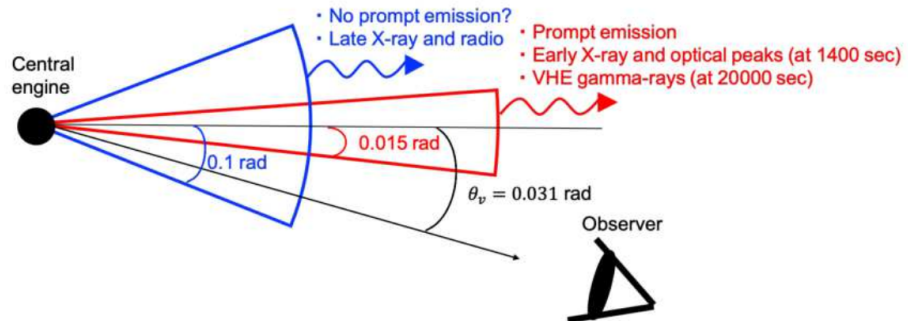


Figure 1. Schematic view of our two-component jet model for GRB 190829A. The red and blue cones represent narrow and wide jets, respectively. Initial shapes of the jets are depicted with their initial opening half-angles. The black arrow shows the observer's line of sight. As the jets expand, they spread sideways, and at $\sim 2 \times 10^4$ s when H.E.S.S. detected VHE gamma-rays, the observer's line of sight is inside the cone of the narrow jet.

- 窄喷流成分主要解释~1400s的X射线和光学余辉的拐折

1.4×10^2 s. We adopt $\theta_v = 0.031$ rad, $\theta_0 = 0.015$ rad, $E_{\text{iso,K}} = 4.0 \times 10^{53}$ erg, $\Gamma_0 = 350$, $n_0 = 0.01 \text{ cm}^{-3}$, $\epsilon_e = 0.2$, $\epsilon_B = 5.0 \times 10^{-5}$ and $p = 2.44$. The initial opening half-angle is small, so that we refer to “narrow jet” in the following. Solid lines in the left panel of Fig. 2 show our results. Our off-axis afterglow model well explains the observational results of early X-ray and optical afterglow from about 8×10^2 to 2×10^4 s. An achromatic behavior in the X-ray and optical

- 宽成分主要解释后期的射电和X射线光变

of the narrow jet are the same as those given in § 3.1. For the wide jet, we adopt $\theta_0 = 0.1$ rad, $E_{\text{iso},K} = 2.0 \times 10^{53}$ erg, $\Gamma_0 = 20$, $\epsilon_e = 0.4$, $\epsilon_B = 1.0 \times 10^{-5}$, and $p = 2.2$. The values of θ_v and n_0 are common for both jets. It is assumed that the central axes of the two jets are identical ($\theta = 0$: see Fig. II).

One can find in the right panel of Figure 2 that early achromatic peaks in the X-ray and optical bands are explained by the off-axis narrow jet emission (dashed lines in the right panel), and that the late X-ray and radio afterglow is interpreted with the wide jet emission (dotted lines). As

- 双成分瞬时辐射, [Chand,2020,url](#)

- VHE E_γ ?

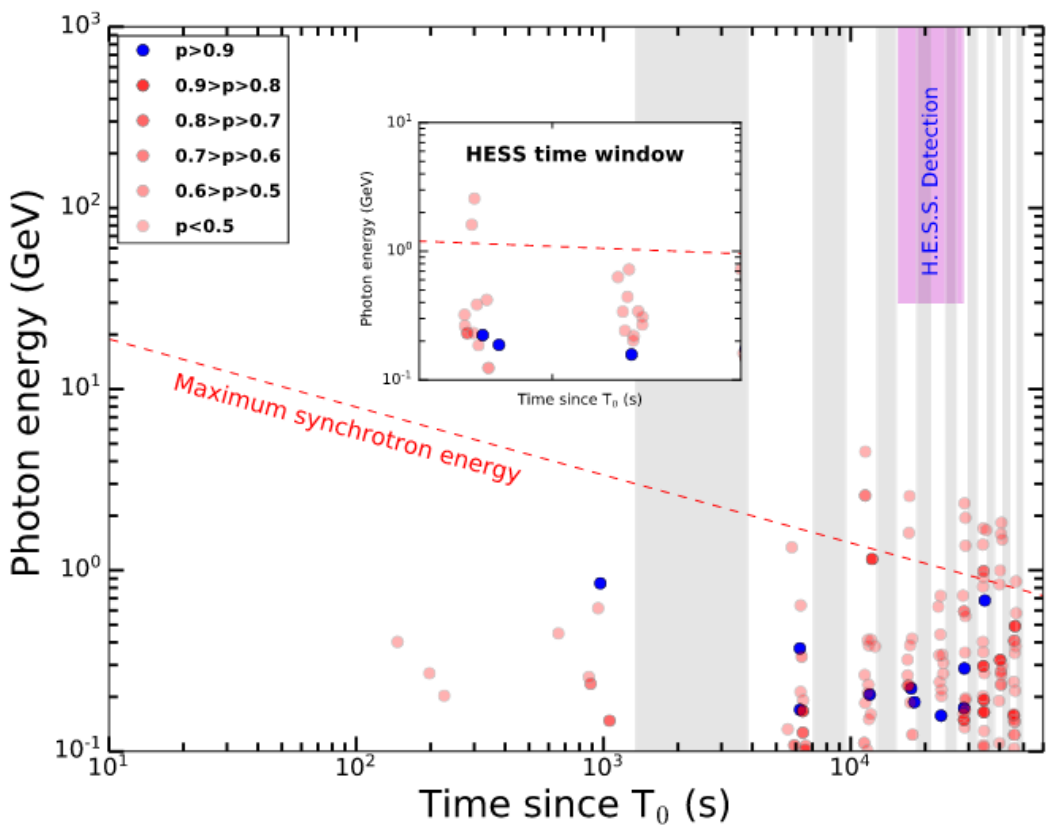


Figure 3. Delayed emission in LAT: all the photons with energies >100 MeV and probabilities of being associated with GRB 190829A. The regions with zenith angle $>100^\circ$ are shaded gray. The red line represents the maximum photon energies allowed for a synchrotron forward-shock model with an emission efficiency $\eta = 1.3\%$. The inset shows the LAT emission during the H.E.S.S. time window.

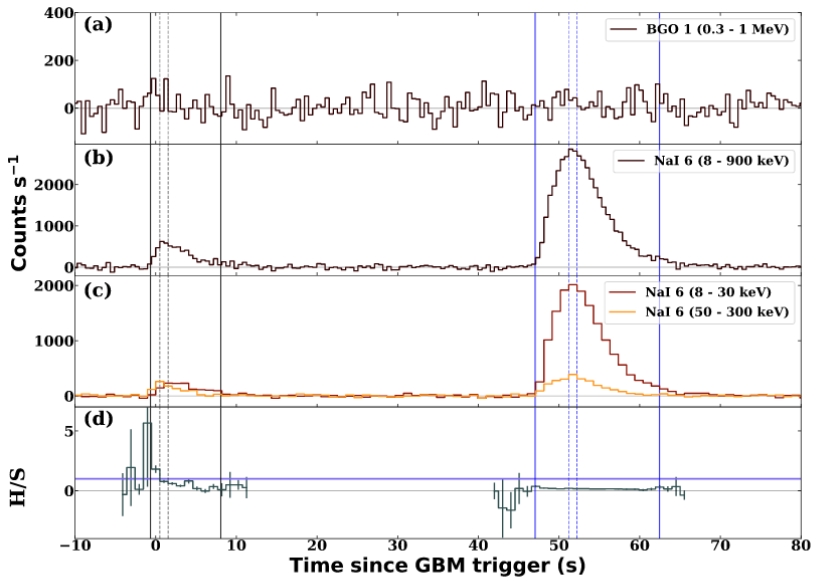


Figure 1. Multichannel light curves: the background-subtracted count rate of GRB 190829A with time in multiple energy bands (a)–(c). (d) The hardness ratio (H/S) in energy bands 50–300 keV (H) and 8–30 keV (S) is shown. The horizontal violet line indicates equal rates in H and S bands. The vertical black and blue lines indicate the boundaries of T_{90} (solid lines) and peak luminosity (dashed lines) calculations for the first and second emission episodes, respectively.

The fast evolving type Ib Supernova SN 2015dj in NGC 7371

<https://arxiv.org/abs/2101.09430>

► details

Authors: Mridweeka Singh, Kuntal Misra, Stefano Valenti, et al.

Comments: 16 pages, 11 figures, accepted for publication in ApJ

We present the detailed optical evolution of a type Ib SN 2015dj in NGC 7371, using data spanning up to ~ 170 days after discovery. SN 2015dj shares similarity in light curve shape with SN 2007gr and peaks at $M_V = -17.37 \pm 0.02$ mag. Analytical modelling of the quasi bolometric light curve yields $0.06 \pm 0.01 M_\odot$ of ^{56}Ni , ejecta mass $M_{ej} = 1.4^{+1.3}_{-0.5} M_\odot$, and kinetic energy $E_K = 0.7^{+0.6}_{-0.3} \times 10^{51}$ erg. The spectral features show a fast evolution and resemble those of spherically symmetric ejecta. The analysis of nebular phase spectral lines indicate a progenitor mass between $13\text{--}20 M_\odot$ suggesting a binary scenario.

- 讨论了Ib型 SN2015dj (宿主星系NGC7371, $D_L = 36.69 \pm 0.05 Mpc$, $z = 0.0090$) 直到发现后170天的光学波段演化。
- 其光变曲线与 SN2007gr 相似，峰值星等 $M_V = -17.32 \pm 0.02$ mag。
- 准热光变曲线的模型拟合给出 $^{56}\text{Ni}: 0.06 \pm 0.01 M_\odot$, $M_{ej} = 1.4^{+1.3}_{-0.5} M_\odot$, $E_K = 0.7^{+0.6}_{-0.3} \times 10^{51}$ erg。
- 光谱特征演化较快，与球对称外流情形相似。
- 星云阶段谱线分析显示前身星质量为 $13\text{--}20 M_\odot$ ，有可能是一个双星。

-
- 如何发现？跟踪观测情况？如何证认为Ib型SN？
 - 如何与SN2007gr相似，有何含义？
 - 如何计算准热光度？
 - 哪些光谱特征演化较快？外流形状如何影响光谱演化？
 - 如何分析星云阶段光谱？
 - 为何 $13\text{--}20 M_\odot$ suggests 双星前身星而不是大质量恒星？
-

- 发现与证认

SN 2015dj (R.A. $22^h 46^m 05.04^s$ and Dec. $-10^d 59^m 48.4^s$) was discovered by Koichi Itagaki on 2015 July 10.655 (UT) in the galaxy NGC 7371, at an unfiltered magnitude of 16.7 mag. The SN was located $19''$ east and $16''$ north of the center of NGC 7371¹.

[see reference](#)

- 开始认为是IIb型超新星，后来分类为Ib型。

a type IIb (SN 2000H) and several type Ib events. The absorption feature at $\sim 6160\text{\AA}$ in the classification spectrum was probably identified in SNID and GELATO as the high velocity absorption component of H α , commonly found in the early spectra of type IIb SN. However, the absence of a discernible H β feature in the classification spectrum suggests that the feature rather corresponds to Si II 6355 \AA . Since Si II 6355 \AA is prevalent in the early spectrum of type Ib SNe, we conclude that SN 2015dj is indeed a type Ib event.

- 跟踪观测情况, see table1 and table2

The photometric and spectroscopic follow up of SN 2015dj initiated soon after discovery and lasted ~ 170 days, mostly obtained through the Las Cumbres Observatory (LCO, Brown et al. (2013)) Supernova Key Project. The photometry was done with the 1m LCO telescopes and the spectroscopy was done with the FLOYDS spectrograph on the 2m LCO telescopes. Additional observations were done with the 1.82m Copernico telescope (Asiago, Italy) and the 2.56m Nordic Optical Telescope (NOT). Broadband $BVgriz$ filters and grisms in the wavelength range of 3300–10000 \AA were used in the observational campaign of SN 2015dj.

- see data reduction section

The LCO photometry was performed using the `lcogtsnpipe` pipeline (Valenti et al. 2016). Since the SN is located close to the host galaxy, template subtraction was adopted to estimate the true SN magnitude after removing the host galaxy contamination. The templates were observed on 2016 June 6 and June 18 in *BVgr* and *i* bands respectively using 1m LCO telescopes, which is approximately 1 year after the explosion. Since the SN could be detected with 1.82 m Copernico telescope on a later date (2016 August 08), we have included the upper limits on the SN magnitudes for the LCO template images in Table 3. The image subtraction was performed using PyZOGY (Guevel & Hosseinzadeh 2017) on LCO data. The 1.82 m Copernico telescope and the 2.56 m NOT data were processed within the IRAF² environment and the instrumental magnitudes were derived from the point spread function photometry using DAOPHOT2 (Stetson 1987). The images taken on 2018 October 01 in *BVgriz* bands with 2.56m NOT were used for template subtraction of the images acquired with 1.82m Copernico telescope and 2.56m NOT following the method described in Singh et al. (2019).

- 提到了一个图像相减的python包[PyZOGY](#),原理,方法有别与Alard&Lupton, 值得研究一下。
- 最后说到的Singh et al. (2019)这篇[文章](#)没有提到如何做图像相减。

- 与SN2007gr光变曲线的整体趋势都相似，没有提到有何含义

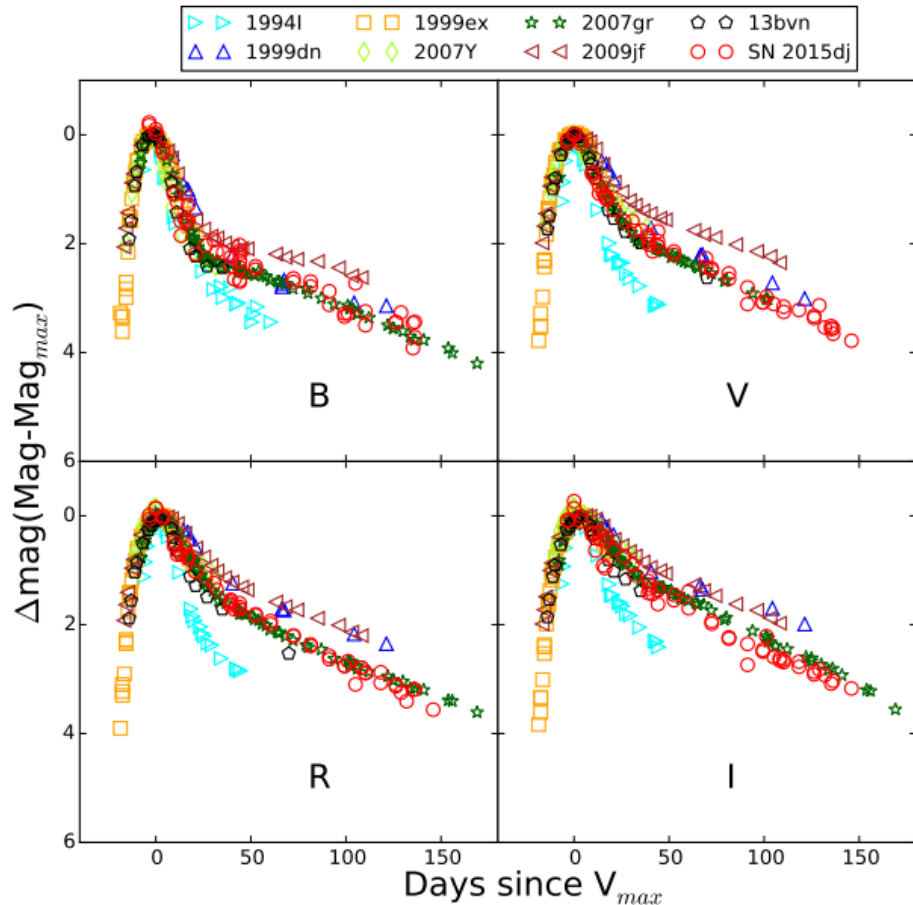


Figure 3. Comparison of light curves of SN 2015dj with other type Ib/Ic SNe. The X-axis is the time from the V -band maximum, the Y-axis is the apparent SN magnitudes normalized to their magnitude at maximum.

- 使用BVRI波段星等计算准热光变曲线

We construct the pseudo-bolometric light curve of SN 2015dj using the extinction corrected magnitudes in the $BVRI$ bands and the luminosity distance (see Sec-

- 星云阶段谱线无偏->球对称外流。即外流形状会影响谱线红移或蓝移

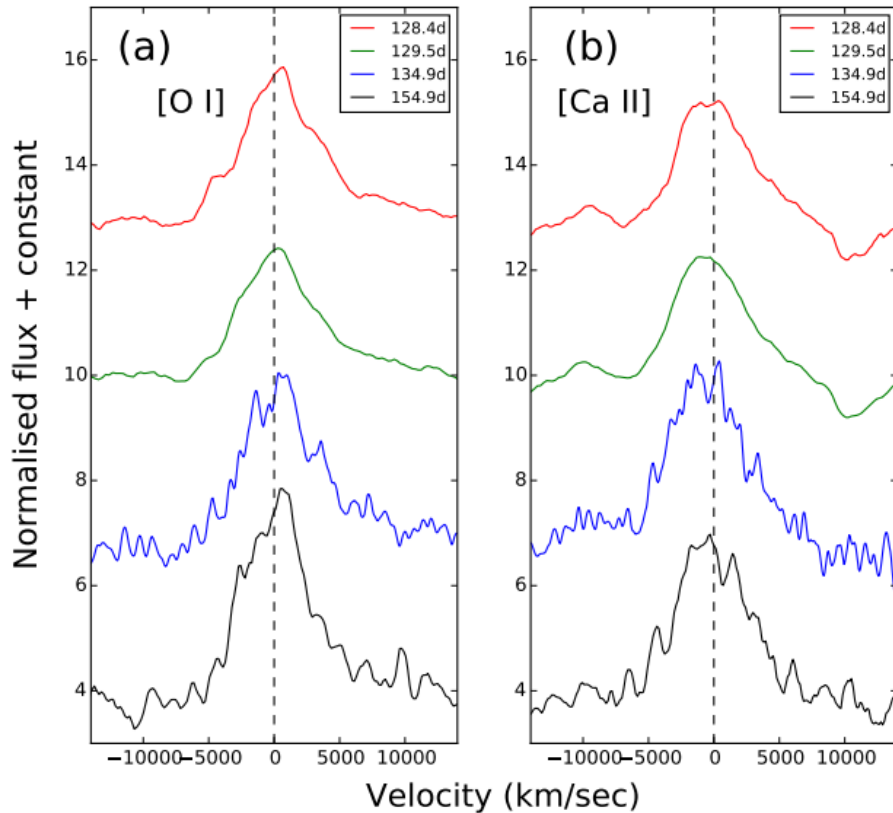


Figure 10. Evolution of the nebular [O I] and [Ca II] line profiles in SN 2015dj.

One of the strongest emission features in type Ib SN nebular spectra is the [O I] doublet at 6300 and 6363 Å. This doublet provides an observational display of the explosion geometry along with other prominent features such as [Ca II] and Mg I]. The [O I] feature is relatively isolated, whereas [Ca II] and Mg I] lines are blended with other lines. Figure 10 (panel a) illustrates the evolution of the [O I] line emission, whose peak shows a negligible shift from the rest wavelength in the velocity space: this is usually interpreted as an indication of spherically symmetric ejecta (Taubenberger et al. 2009).

Figure 10 (panel b) presents the evolution of the [Ca II] doublet 7291, 7324 Å. It has a flat peak likely due to line blending. The strength of the [Ca II] feature increases with time. Calcium clumps formed during explosion do not contribute considerably to the [Ca II] emission (Li et al. 1993; Matheson et al. 2000). This feature is produced by the excitation of calcium present in the atmo-

sphere by the pre-existing envelope. No evident shift from the rest velocity is observed for this emission feature, supporting spherical symmetry in the matter ejection (Figure 10, panel b)).

- 偏移谱线的例子：[2101.11340](#)

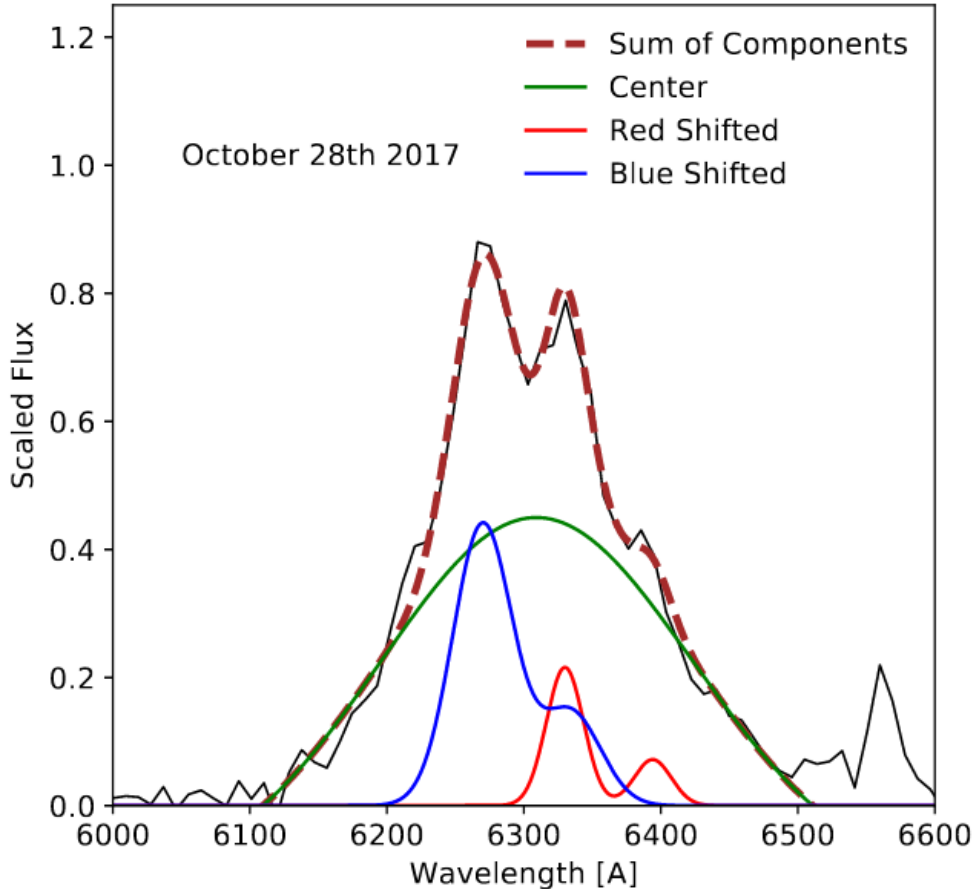


Figure 9. Fits to the [O I] $\lambda\lambda 6300, 6363$ doublet for the October 28th 2017 spectrum of SN 2017ein using the same method as in Taubenberger et al. (2009). The region around the doublet is normalised and scaled before the fit is applied.

sians comprised of a red and blue shifted blob and a central blended feature. We find a redshifted blob at a velocity shift of -1200 km s^{-1} and a blueshifted blob at a velocity shift of 2000 km s^{-1} . From Taubenberger et al. (2009), a combination of these three components best reflects an asymmetric ejecta.

- 由此看似乎本文的判断不够严谨。
- 由星云阶段 O I 线推断前身星质量为 $15-20 M_{\odot}$

$$M_O = 10^8 \times D^2 \times F_{[O I]} \times e^{(2.28/T_4)} \quad (1)$$

$T_4 = 0.4$. The observed flux of the [O I] line doublet at 155 days is 2.10×10^{-14} erg s $^{-1}$ cm $^{-2}$; adopting a distance of 36.69 ± 0.05 Mpc, we infer oxygen mass of $0.85 M_{\odot}$.

plosion. The [O I] emission is produced because of a layer of oxygen formed during the hydrostatic burning phase. This oxygen mass is correlated with the main sequence progenitor mass (Thielemann et al. 1996). Following (Thielemann et al. 1996) we thus estimate the progenitor and the He core masses to be $15\text{--}20 M_{\odot}$ and $4\text{--}8 M_{\odot}$, respectively.

- 另一方面，经过与不同前身质量的核合成模型比较，显示该SN前身星质量约为 $13M_{\odot}$ ，故得出 $13\text{--}20M_{\odot}$

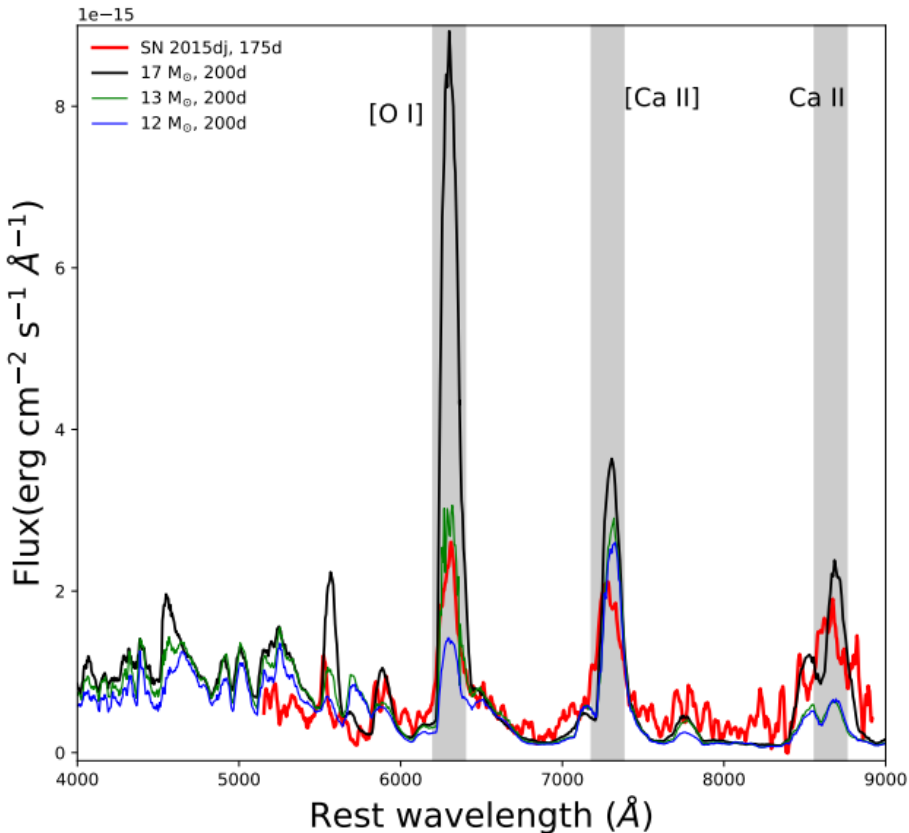


Figure 11. Comparison of the late nebular spectrum of SN 2015dj with models of Jerkstrand et al. (2015) having different progenitor masses. Models have been scaled to match the properties of SN 2015dj in terms of [O I] luminosities.

We compare the spectrum of SN 2015dj with the 200 days post explosion model spectra of Jerkstrand et al. (2015) having progenitor masses of 12, 13 and $17 M_{\odot}$ (Figure 11). These models were produced for a ^{56}Ni mass of $0.075 M_{\odot}$ and a distance of 7.8 Mpc. The flux calibrated spectrum at ~ 175 day after explosion (155 day since V_{max}) of SN 2015dj is corrected for redshift and reddening. The model spectrum is scaled to match the ^{56}Ni mass, distance and corresponding phase of SN 2015dj. We find that the luminosity of the [O I] feature of SN 2015dj is similar to $13 M_{\odot}$ progenitor star.

- 为何认为是双星前身星？

Moreover, the flux ratio of [O I] and [Ca II] lines can serve as a tool to probe the progenitor mass. Kun-

itors in binary systems. In type Ib/Ic SNe, this ratio is in the range \sim 0.9 - 2.5, whereas in type II SNe it is < 0.7 (Kuncarayakti et al. 2015). In SN 2015dj, the [O I]/[Ca II] flux ratio is between 0.72 and 0.86 inferred from the spectra at 128 and 155 days respectively. This flux ratio is in between the quoted values for type II and

Ib/Ic SNe and indicates the association of SN 2015dj with a lower mass progenitor in a binary system.

- 为何质量在这之间的是双星 ? [Kuncarayakti 2015](#)

We also measured the line ratio of [O I] $\lambda\lambda$ 6300, 6364/[Ca II] $\lambda\lambda$ 7291, 7324 emissions in the nebular spectrum of iPTF13bvn and compared it to other stripped-envelope SNe, as well as several Type-II SNe taken from the SUSPECT⁴ Online Supernova Spectrum Archive. This line ratio is known to be insensitive to the density and temperature, while increases with increasing progenitor mass (Fransson & Chevalier 1989; also see

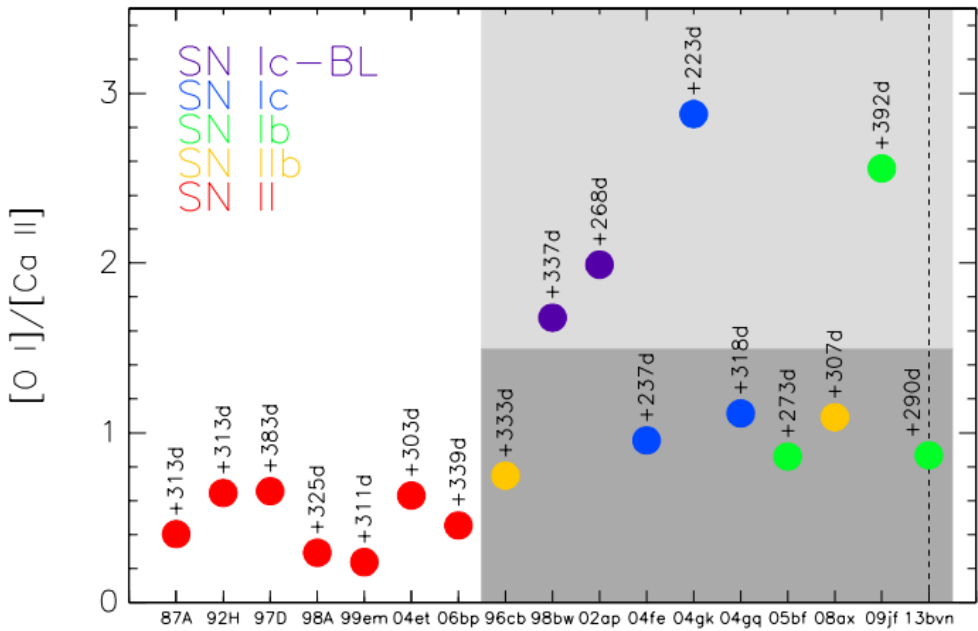


Fig. 7. $[\text{O I}]_{\lambda\lambda 6300,6364}/[\text{Ca II}]_{\lambda\lambda 7291,7324}$ line ratio of several core-collapse SNe of similar ages during the nebular phase. Red symbols indicate SN Type-II, orange Type-IIb, green Type-Ib, blue Type-Ic, and purple broad-lined Type-Ic. The SN phases with respect to the time of maximum light are shown next to the each data point and the dashed vertical line indicates iPTF13bvn. The light-grey shaded region indicates the single star progenitors and the dark-grey shaded region indicates the binary progenitors for Type-Ib/c SNe. The exact border between these two regions is unknown, thus arbitrarily taken at $[\text{O I}]/[\text{Ca II}] = 1.5$ in this plot for the purpose of indicating the two distinct populations. References for the spectra of individual SNe: 1987A

This spread may be interpreted as indicating the presence of two different populations of SNe Ib/c (shaded regions in Fig. 7), i.e. those coming from massive single Wolf-Rayet progenitors, and lower-mass progenitors in binary systems (Kuncarayakti et al.

Exploring the diversity of double detonation explosions for type Ia supernovae: Effects of the post-explosion helium shell composition

<https://arxiv.org/abs/2101.09792>

► details

Authors: M. R. Magee, K. Maguire, R. Kotak, S. A. Sim

Comments: 21 pages, 25 figures, 1 table. Accepted for publication in MNRAS. Model light curves available at [this URL](https://arxiv.org/abs/2101.09792)

The detonation of a helium shell on top of a carbon-oxygen white dwarf has been argued as a potential explosion mechanism for type Ia supernovae (SNe~Ia). The ash produced during helium shell burning can lead to light curves and spectra that are inconsistent with normal SNe~Ia, but may be viable for some objects showing a light curve bump within the days following explosion. We present a series of radiative transfer models designed to mimic predictions from double detonation explosion models. We consider a range of core and shell masses, and systematically explore multiple post-explosion compositions for the helium shell. **We find that a variety of luminosities and timescales for early light curve bumps result from those models with shells containing ^{56}Ni , ^{52}Fe , or ^{48}Cr . Comparing our models to SNe~Ia with light curve bumps, we find that these models can reproduce the shapes of almost all of the bumps observed, but only those objects with red colours around maximum light ($B-V \gtrsim 1$) are well matched throughout their evolution.** Consistent with previous works, we also show that **those models in which the shell does not contain iron-group elements provide good agreement with normal SNe~Ia of different luminosities from shortly after explosion up to maximum light.** While our models do not amount to positive evidence in favour of the double detonation scenario, we show that provided the helium shell ash does not contain iron-group elements, it may be viable for a wide range of normal SNe~Ia.

考虑不同的核质量和壳层质量，以及一系列不同的壳层化学成分，可以模拟出不同的双爆轰情形下的超新星光变。(有bump的，普通的)

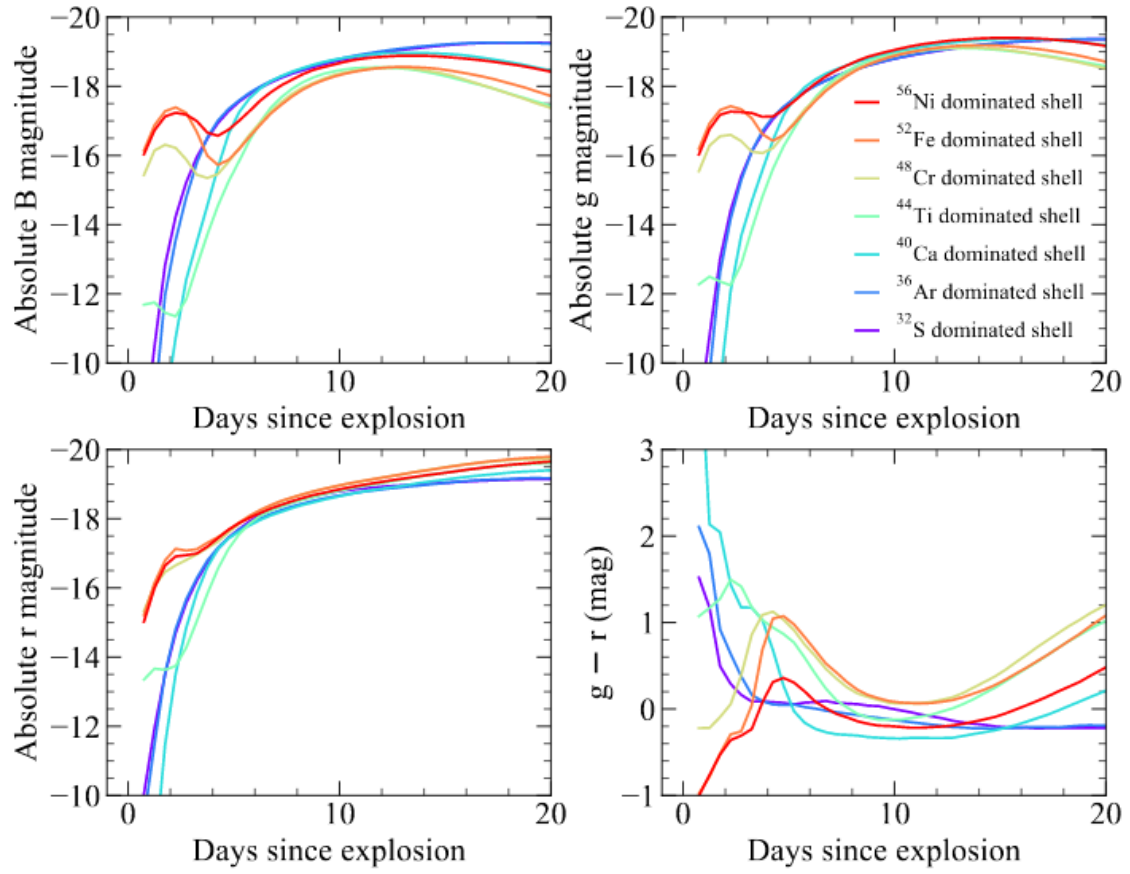


Figure 5. Light curves and colours for models with different shell compositions. All models shown have a $1.0 M_{\odot}$ core and a $0.07 M_{\odot}$ shell, of which 50% is burned to elements heavier than helium. The dominant α -chain product produced in the shell is given by the colours. The relative fractions of all other isotopes in the shell are given following from Fig. 4.